DESIGNING LOW FREQUENCY BAND GAPS IN ADDITIVELY MANUFACTURED PARTS USING INTERNAL RESONATORS

Waiel Elmadih[1], Wahyudin P. Syam[1], Ian Maskery[2], Richard Leach[1]
[1]Manufacturing Metrology Team
[2]Centre for Additive Manufacturing
University of Nottingham
Nottingham, NG8 1BB, UK

INTRODUCTION

Additive manufacturing technologies provide a high degree of design freedom to exploit complex structures with tailorable mechanical properties. Within these properties lies vibration isolation, which depends mainly on the mass and stiffness of the structure. Traditional techniques for providing vibration isolation promote shifting the resonant frequency above or below the frequency of interest [1–3]. There has been little focus on methods to completely eliminate vibration waves from a precision engineering component. One promising method to do this is to design the structure to have a phononic band gap (BG) spanning the frequency of the undesirable incident waves [4]. A BG is a frequency region in which there is no propagation of elastic waves [5].

BGs can be formed by Bragg scattering or through the use of internal resonators. A Bragg scattering BG is formed by the destructive superposition of reflected waves, and occurs at frequencies of the order of the wave speed divided by the size of the unit cell of which the structure is composed [6]. Several applications of Bragg BGs have been reported successful as can be seen in the work of Ampatzids et al. [7] who presented and experimentally verified a 1D BG at sub-7 kHz in composite material. Hsu et al. [8] presented a silicon-based metametrial with several BGs between 60 MHz and 100 MHz, and Wang et al. [9] proposed a 3D periodic structure with a BG between 35 MHz and 36 MHz. Bragg induced BGs can also be seen in the work of Martin et al. [10]. The main difference between internal resonator band gaps (IRBs) and Bragg scattering BGs is that IRBs can be tuned to much lower frequencies, by hindering the wave propagation around the resonance of the structure. Liu et al. [11] presented a 3D structure including lead spheres embedded in a soft rubber coating; that structure provided an IRB with a response lower by two orders of magnitude than the reference structure of no IRB mechanism. Matlack et al. [12] designed additively manufactured lattice structures with embedded resonators and recorded IRBs in frequency ranges between 2.4 kHz and 8.3 kHz [12].

In this paper, we report on the design, modelling and experimental verification of a repeating lattice structure with a tuneable low frequency BG based on internal resonators. We present relationships between the BG properties and the geometrical parameters of the proposed IRB structure. An optimised IRB structure is then used in a case study in which a vibration isolation platform is designed to provide isolation for an all-optical dimensional measuring system (AODMS) [13]. The control of IRBs will serve as a future design tool for machines and structures with elimination of vibration waves in multiple degrees of freedom.

THE IRB UNIT CELL

The general IRB unit cell of this study is shown in FIGURE 1. The outer frame is a scaffold providing structural integrity, whilst a resonator occupies the centre of the cell and connects to the scaffold walls with six thin struts.

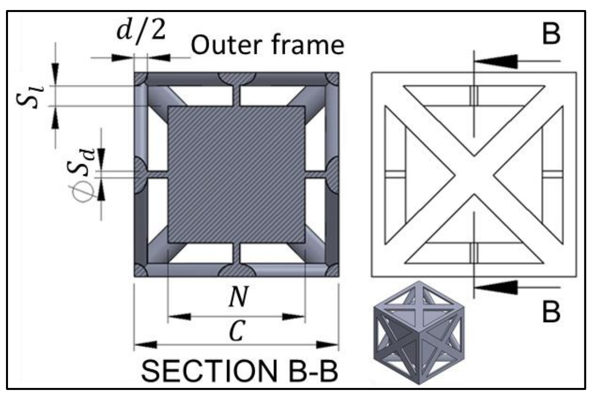

FIGURE 1. IRB unit cell. The outer frame supports structural loads, while the lower stiffness struts (with thickness S_d and length S_l) and resonator (of dimension N) hinder wave propagation and provide a tunable BG.

The various cell dimensions are related by

$$C = N + 2S_l + d \tag{1}$$

where C is the cell size, S_l is the length of an internal strut, N is the length of the resonator and d is the diameter of the struts making up the supporting scaffold. The reader is referred to the design tool in reference [2] for information on designing strut-based lattices of different volume fractions and sizes.

METHODOLOGY

The IRB unit cell of this study can be tessellated in 3D using the linear lattice vectors $n_1e_1 + n_2e_2 + n_3e_3$. The periodicity of the lattice structure can be defined in the spatial coordinates as

$$\begin{aligned} e_x &= C_x i_x, \\ e_y &= C_y i_y, \\ e_z &= C_z i_z, \end{aligned} \tag{2}$$

where $e_{x,y,z}$ are the lattice basic vectors, $C_{x,y,z}$ are the unit cell sizes and $i_{x,y,z}$ are the lattice periodicity numbers. For a cubic lattice, C_x, C_y and C_z are all equal to C.

This work uses a finite element (FE) method which can predict BGs with higher accuracy and efficiency [12,14] than the wavelet method [15], plane wave expansion method [16] and finite difference time domain method [17]. The FE method also allows the calculation of the dispersion curves (DCs) of complex structures, such as the IRB unit cell of this study. For modelling the elastic wave propagation, the reciprocal lattice vectors (k_x, k_y and k_z) for the cubic IRB lattice of study can be expressed by

$$\begin{aligned} k_x &= \frac{2\pi}{C_x} i_1, \\ k_y &= \frac{2\pi}{C_y} i_2, \\ \text{and} \qquad k_z &= \frac{2\pi}{C_z} i_3. \end{aligned} \tag{3}$$

Bloch theorem dictates that the propagation of waves in a periodic structure can be understood by the harmonic displacement of a single unit cell [6]. In our case, we have

$$\boldsymbol{q_1} = e^{-i\omega k} \boldsymbol{q_2} \tag{4}$$

where $\boldsymbol{q_1}$ and $\boldsymbol{q_2}$ represent the displacements of the nodes at one edge or face of the unit cell, and ω is their angular frequency. The vectors k are bounded by a single reciprocal lattice unit cell [6]. Within this reciprocal cell, k values are further restricted to only part of the reciprocal cell called the irreducible Brillouin zone (IBZ), as shown in FIGURE 2. The IBZ contains sufficient wavevectors to describe wave propagation throughout the whole structure.

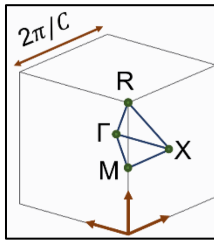

Γ(0,0,0)	X(π/C,0,0)
M($\pi/C, \pi/C$,0)	R($\pi/C, \pi/C, \pi/C$)

FIGURE 2. The IBZ of a cubic lattice. On the right are the reciprocal space coordinates (k_x, k_y, k_z) for a set of commonly examined wavevectors.

For a cubic lattice, we identify three types of nodes (see FIGURE 3) in the 1D case and thus three vectors containing the displacements of the cell are considered: the leftmost nodes, rightmost nodes and all inner nodes. The number of nodes expands to nine in 2D, and nineteen in 3D, which is the focus of this work.

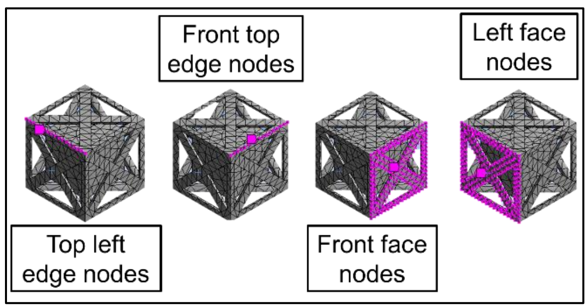

FIGURE 3. Examples of the types of nodes in the proposed IRB cell.

A generalised eigenvalue problem

$$\boldsymbol{K} - \omega^2 \boldsymbol{M} = 0 \tag{5}$$

is constructed for each wavevector in the IBZ, based on stiffness and mass matrices obtained from the commercial software ANSYS (after ensuring mesh convergence). The scan for the eigenvalues is carried out in four runs along the Γ-X, X-M, M-R, and R- Γ directions, and the total count of wavevectors representing the IBZ is set to 360. Frequency regions with no solution for the eigenvalue problem indicate BGs.

In this investigation, the ratio S_d/c is varied, taking values between 0.005 and 0.033, and the wavevector DCs are calculated at each value. The same commercial software (ANSYS) is used to model the attenuation profile of a structure with a finite number of IRB cells. Experimental verification is provided by additively manufacturing a structure of similar number of unit cells from Nylon-12 with laser powder bed fusion (LPBF), then performing a vibration test.

RESULTS AND DISCUSSION

We present the calculated DCs of an IRB cell with the parameters S_l/c = 0.1, S_d/c = 0.033, and C= 30 mm. The material properties for Nylon-12 parts manufactured with LPBF are presented in TABLE 1 and the DCs are shown in FIGURE 4.

TABLE 1. Properties of L-PBF Nylon-12 [18].

Density	Young's modulus	Poisson's ratio
0.95 g/cm^3	1500 MPa	0.35

Wavebands which start to propagate at 0 Hz are interrupted with a BG caused by the internal resonator at 1620 Hz. The BG spans across the four selected boundaries of the IBZ, Γ-X-M-R-Γ and thus it is a 3D BG. The BG continues up to 2700 Hz where new wavebands start propagating.

The ability of this unit cell to provide vibration isolation between 1620 Hz to 2700 Hz is confirmed by examining a structure of the same unit cell in 9×9×9 tessellations. According to Chen et al. [19], any number of unit cells higher than seven is enough to identify a BG with harmonic response analysis. The leftmost nodes are excited with a harmonic force of 1 N between 0.1 Hz to 3500 Hz with a sample spacing of 1 Hz. The average displacement of all rightmost nodes of the structure under the aforementioned settings are depicted in FIGURE 4 (inset). It is observed that the displacement is attenuated in the BG region between 1620 Hz to 2700 Hz. The frequency can be normalised with the speed of the wave in the medium v and the cell size C to provide more generalised results. This gives the advantage of adding the material and the cell size to the BG tuning mechanism. Thus, the right ordinate of FIGURE 4 and the abscissa of FIGURE 4 (inset) show the normalised frequency for the unit cell under study. The normalised frequency of the BG is calculated to be from 0.039 to 0.065.

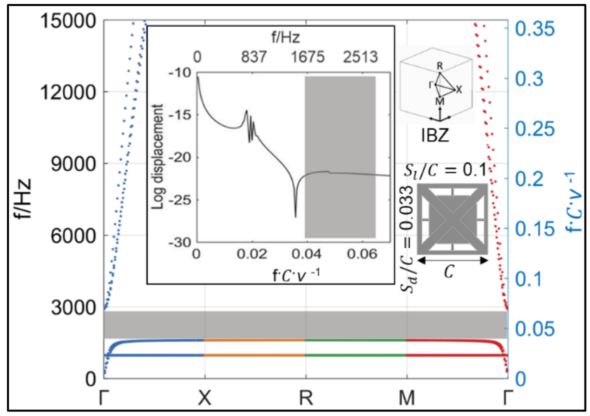

FIGURE 4. DCs of a cubic IRB lattice cell and harmonic response analysis of the same cell in 9×9×9 tessellations (inset). Wave propagation is shown along selected reciprocal vectors in the IBZ. The shaded frequency region represents a 3D BG.

Bandgap tuning parameter

For control of the BG in FIGURE 4, a structural parameter identified as the ratio between the diameter of the resonator strut to the cell size S_d/C is selected because it is expected to have a direct control on the stiffness of the resonator. Having control over the stiffness of the resonator is the first step towards tuning the stiffness/mass ratio (K/m) and tuning the ability of the cell to provide a BG. S_d/C takes values in the range of 0 to $1-d/C$. The parameter d/C takes a value of 0.13 for a 30% volume fraction cell [2]. Thus, the identified parameter S_d/C takes values between 0 and 0.87.

Since our interest is low frequency BGs (see Case study section), we choose S_d/C values in the lower range, as can be seen in TABLE 2. Values in this lower range are expected to provide a low K/m ratio of the resonator mechanism and ultimately a low resonance frequency.

The starting value S_d/C = 0.033 is selected with the aim of designing an IRB cell with unit cell size of 30 mm and a resonator strut of a diameter equal to the minimum LPBF manufacturing size (1 mm). To ensure that the mass of the IRB cell is kept constant, the study is carried at a constant S_l/C value of 0.1. This value is aimed at having a high value of m for the resonator to ensure a lower resonant frequency while ensuring low overhang of the struts to avoid lamination during LPBF.

TABLE 2. *The parameters of five unit cells used in the BG tuning study.*

S_l/C \ S_d/C	0.1
0.033	Start and end normalised frequencies of the BG formed by any combination of these values are calculated and are shown in FIGURE 4.
0.025	
0.02	
0.01	
0.005	

It is assumed that at S_d/C = 0, the resonator has no diameter, and thus no IRB mechanism is available. The normalised start and end frequencies as calculated for the five IRB cell types are given in FIGURE 5. All the cells provided BGs.

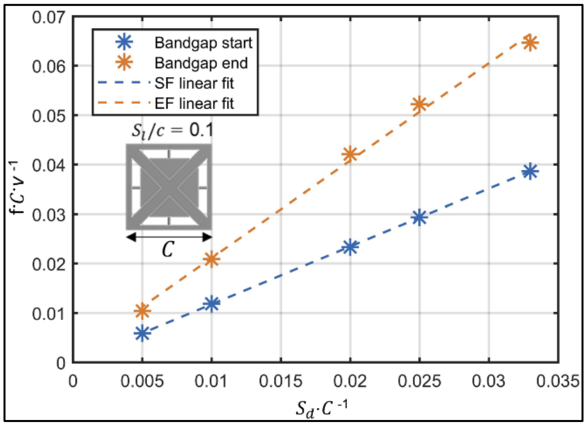

FIGURE 5. The lower and upper normalised BG frequencies for various configurations of IRB cell (see TABLE 2).

The lowest recorded BG spanned a normalised frequency range from 0.005 to 0.01. This was for the cell of S_d/C=0.005. This BG was the narrowest compared to those of the other examined cells. The start and end frequencies of the BG increase linearly with the increase in S_d/C. The equation that correlates the parameter S_d/C to the normalised BG start frequency (SF) is

$$SF = (1.17 \pm 0.013)\frac{S_d}{C} + 3.7 \times 10^{-5} \pm 0.001, \quad (6)$$

which is a linear fit to the numerical data of SF with an adjusted *R*-squared value of 0.9999. The equation that correlates the parameter S_d/C to the normalised BG end frequency (EF) is

$$EF = (1.97 \pm 0.205)\frac{S_d}{C} + 13.97 \times 10^{-4} \pm 0.004, \quad (7)$$

which is a linear fit to the numerical data of EF with an adjusted *R*-squared value of 0.9947.

Experimental verification

Using LPBF, a 3×3×3 Nylon-12 sample with a cell size of 30 mm was fabricated. Due to the 1 mm manufacturing limitation of the employed LPBF system, the nominal strut diameter was designed to be 1 mm, and the strut length was 3 mm. The strut diameter was manufactured with a deviation of -10% from the nominal value. The targeted mass was 297 g, while the measured mass was 350 g. This deviation is expected to be due to changes in material density related to the laser scanning speed, powder quality and laser power of LPBF system. The experiment set up is shown in FIGURE 6.

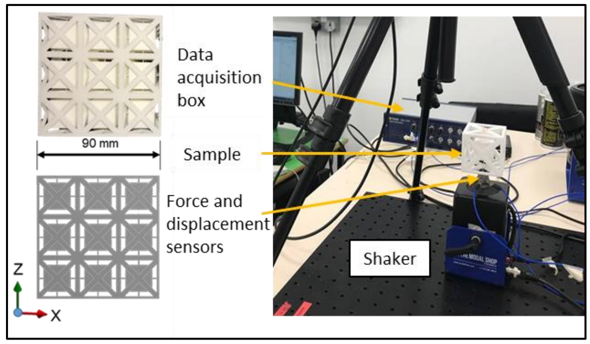

FIGURE 6. 3×3×3 *Nylon-12 sample as modelled (bottom left) and fabricated (top left). The experimental setup is shown on the right.*

A periodic chirp excitation signal is send through the data acquisition box to the Modal Shop K2007E01 shaker. The signal bandwidth was 0 kHz to 3.5 kHz. The sample is attached to force and displacement sensors which are in turn attached to the shaker. The experiment was controlled using proprietary software which controls a data acquisition box, to which the shaker and oscillation sensors are attached. The experimental result, shown in FIGURE 7, is produced with multiple sweeps of the frequency range with a sample spacing of 0.39 Hz.

The experiment is in good agreement with the simulation of similar settings in terms of resonant frequencies, general attenuation profile and lack of resonance peaks in the BG frequency region.

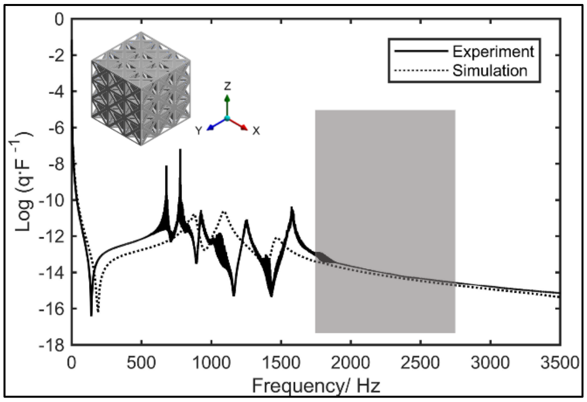

FIGURE 7. Harmonic response analysis of 3×3×3 Nylon-12 sample as simulated (dotted line) and experimentally tested (solid line). The ordinate shows the logarithm of the displacement q per unit input force F.

CASE STUDY

A metrology platform is to be designed using IRB lattice structures to provide 3D vibration isolation in the range between 50 Hz to 100 Hz. The dimensions of the required platform are: min. (150×150×150) mm, max. (200×200×200) mm for an AODMS sensor of 10 kg mass. The aim of the study is to determine whether IRB structures are suitable for providing the isolation in the specified range.

Results and discussion

The first step was to select the IRB cell that can provide the BG within the specified frequency region. The selection was made by searching for the BG by the input of the material properties and cell size to FIGURE 5. The ability of a specific cell of certain dimensions and material composition to provide a suitable BG was then explored. Unit cells that can provide the BG within the sought frequency region were identified. Two unit cells of different size and material composition that can provide the BG between 50 Hz to 100 Hz are highlighted and the cells' specifications are summarised in TABLE 3.

TABLE 3. IRB cells that can provide vibration isolation between 50 Hz to 100 Hz.

Option	(1) S_d = 0.75 mm S_l = 15 mm 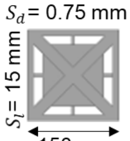 150 mm	(2) S_d = 1 mm S_l = 5 mm 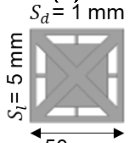 50 mm
Material	Nylon-12	TPE-210-s
Cell mass	1.37 kg	53.8 g
Young's modulus	1.5 GPa	8 MPa

Of these two cells, option-2 is more suitable for manufacturing the platform due to:

- The compact cell size of 50 mm that allows higher number of tessellation in a confined space of (200×200×200) mm and thus better realisation of the BG.
- Larger minimum feature size of 1 mm compared to 0.75 mm for option-1, and thus better suitability for LPBF.
- Higher number of cells, and thus a more defect tolerant design.

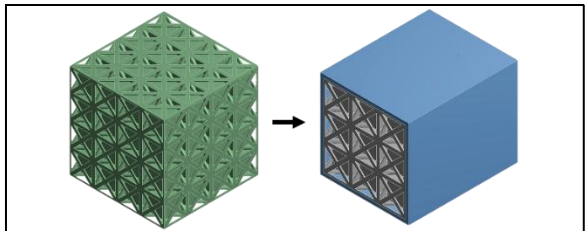

FIGURE 8. Improvements made on the IRB platform design: (b) higher structural stiffness.

The low Young's modulus of option-2 allows the realisation of BGs at low frequencies and with achievable cell dimensions. However, the material suffers from two limitations: low structural stiffness and high thermal expansion coefficient. To address these two issues, the design of FIGURE 8 (b) proposes the use of 3×3×4 IRB cells embedded in solid aluminium casing of 3 mm thickness. The design is modelled to withstand double the mass of the sensor for safety. The simulated responses of the described structure are shown in FIGURE 9 and depict attenuation of the excitation signal between 50 Hz to 100 Hz in 3D.

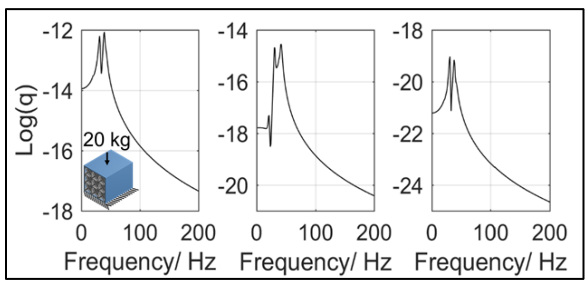

FIGURE 9. Simulated harmonic response of IRB cells with solid Al host in longitudinal (left), x- (middle) and y- (right) directions under 20 kg load.

CONCLUSIONS

We have shown that strut-based lattices can be designed to have low frequency 3D BGs when resonators are embedded within the structure. The strut diameter of the resonator is found to be a direct means for tuning the BG. BGs in frequency regions as low as 50 Hz are predicted to be achievable using a low-stiffness 50 mm lattice cell embedded in an Al casing. Verification of the BG simulation method was carried using a 30 mm Nylon-12 specimen fabricated with LPBF. Good agreement with the simulated results was found. This work is a promising step forward for eliminating vibrations in precision engineering applications. Future work will examine more IRB lattices with more BG tuning parameters, and will study the design and manufacturability of a metrology frame for an AODMS. This work was supported by the Engineering and Physical Sciences Research Council (grant number EP/M008983/1). The authors would like to thank Joseph White from University of Nottingham for helping with this work.

REFERENCES

[1] Syam WP, Jianwei W, Zhao B, Maskery I, Elmadih W, Leach RK. Design and analysis of strut-based lattice structures for vibration isolation. Precis. Eng. 2017; 52: 494-506.

[2] Elmadih W, Syam WP, Maskery I, Leach RK. Additively manufactured lattice structures for precision engineering applications. Proc. 32nd ASPE. Charlotte: 2018.

[3] Schmitz TL, Smith KS. Mechanical vibrations: modeling and measurement. Springer. New York: 2011.

[4] Panesar A, Abdi M, Hickman D, Ashcroft I. Strategies for functionally graded lattice structures derived using topology optimisation for additive manufacturing. Additive Manufacturing. 2018; 19: 81-94.

[5] Elmadih W, Syam WP, Maskery I, Chronopoulos D, Leach RK, Mechanical vibration bandgaps in surface-based lattices. Additive Manufacturing. Under review (2018).

[6] Phani AS. Elastodynamics of lattice materials, in: Phani AS, Hussein M I. Dynamice of lattice material. John Wiley and Sons. 2017; 53–59.

[7] Ampatzidis T, Leach RK, Tuck CJ, Chronopoulos D. Band gap behaviour of optimal one-dimensional composite structures with an additive manufactured stiffener. J. Compos. Part B Eng. 2018; 153: 26–35.

[8] Hsu FC, Lee C I, Hsu JC, Huang TC, Wang CH, Chang P. Acoustic band gaps in phononic crystal strip waveguides. Appl. Phys. Lett.. 2010; 96: 3-6.

[9] Wang L, Bertoldi K. Mechanically tunable phononic band gaps in three-dimensional periodic elastomeric structures. Int. J. Solids Struc. 2012; 49: 2881-2885.

[10] Martin A, Kadic M, Schittny R, Bückmann T, Wegenerz M. Phonon band structures of three-dimensional pentamode metamaterials. Phys. Rev. B. 2017; 025309:1-7

[11] Liu Z, Zhang X, Zhu YY, Yang Z, Chan C T, Sheng P. Locally resonant sonic materials. Science. 2000; 289:1734-1736.

[12] Matlack KH, Bauhofer A, Krödel S, Palermo A, Daraio C. Composite 3D-printed meta-structures for low frequency and broadband vibration absorption. 2016; 113: 8386-8390.

[13] Leach RK, Elmadih W, Piano S, Senin N, Sims-Waterhouse D, Syam WP, Su R, Thomas M. Enriching micro-scale metrology with an all- optical dimensional measuring system. Proc. euspen Micro/Nano Manufacturing Workshop. Strathclyde: 2017.

[14] Khelif A, Hsiao FL, Choujaa A, Benchabane S, Laude V. Octave omnidirectional band gap in a three-dimensional phononic crystal. IEEE Trans. Ultrason. Ferroelectr. Freq. Control. 2010; 57: 1621–1625.

[15] Yan Z, Wang Y, Zhang C. Wavelet method for calculating the defect states of two-dimensional phononic crystals. Acta Mech. Solida Sin. 2008; 21: 104–109.

[16] Zhou XZ, Wang YS, Zhang CS. Three-Dimensional sonic band gaps tunned by material parameters. Appl. Mech. Mater. 2010; 29: 1797–1802.

[17] Sigalas MM, García N. Theoretical study of three dimensional elastic band gaps with the finite-difference time-domain method. J. Appl. Phys. 2000; 87: 3122–3125.

[18] Materialise. PA 12 (SLS): Datasheet. 2018; http://www.materialise.com/en/manufacturing/materials/pa-12-sls (accessed January 31, 2018).

[19] Chen Y, Yao H, Wang L. Acoustic band gaps of three-dimensional periodic polymer cellular solids with cubic symmetry. J. Appl. Phys. 2013; 114: 043521-043528.